CICE 2023 Rio de Janeiro – Brazil 11TH INTERNATIONAL CONFERENCE ON FRP COMPOSITES IN CIVIL ENGINEERING

Fatigue strength and stiffness degradation of the woven roving GFRP under compression-compression cyclic loading

Akihiko Sato, Kyoto University, Japan, sato.akihiko.45m@st.kyoto-u.ac.jp
Yasuo Kitane, Kyoto University, Japan, kitane.yasuo.2x@kyoto-u.ac.jp
Kunitomo Sugiura, Kyoto University, Japan, sugiura.kunitomo.4n@kyoto-u.ac.jp
Hideki Hibi, HIBI Co.,Ltd., Japan, hidekey@hibi-frp.co.jp
Yoshinao Goi, Kyoto University, Japan, goi.yoshinao.2r@kyoto-u.ac.jp

ABSTRACT
This study revealed compression-compression fatigue behavior of woven roving GFRP laminate used in civil structures. Both static compression test and compression-compression fatigue test were conducted. As a result, fatigue failure was observed even in the compression fatigue test. The S-N curve of compression fatigue was similar to those of tensile fatigue, but the compression fatigue test exhibited smaller fatigue strength than tension when fatigue failure occurred at small loading cycles. Moreover, the stiffness measured through the fatigue test revealed that stiffness decreased as the loading cycle increased. Finally, authors proposed the model which can express the stiffness degradation under compression fatigue.

KEYWORDS
Fatigue, S-N curve, Stiffness degradation, Microscope observation

INTRODUCTION
Fiber Reinforced Polymers (FRP) made up of fiber and matrix resin has been widely used in civil structures. The first application to civil structures was repairing and retrofitting of existing structures in 1980s. Carbon-FRP (CFRP) was used for this purpose because it had high strength and stiffness (Bank, 2007). In the same period, attempts were made to use FRP as primary members of bridge structures. Glass-FRP (GFRP) was suitable for this applications because of its cheaper cost than CFRP. Many GFRP bridges have been built from 1980s (Hollaway & Head, 2001). Most of them were pedestrian bridges because GFRP bridges have lower stiffness than bridges of conventional materials. Threrefore, fatigue was not serious problem in GFRP pedestrian bridges (Japan Society of Civil Engineers, 2011). However, recently, short-span GFRP vehicular bridges have been increased in Europe and USA (Behrends & Brayshaw, 2012)(Siwowski et al., 2018). The number of such GFRP vehicular bridges is expected to increase in the future, as many existing short-span bridges are ageing. As the live loads are higher on vehicular bridges than on pedestrian bridges, the authors focused on the fatigue of GFRP.

The fatigue bihaviour of GFRP have been vigorously studied in previous researches. It is known that fatigue strength of GFRP can be expressed by S-N curve in the same way as steel structures, but GFRP does not show a clear fatigue limit until 10 millions loading cycles. (Vassilopoulos & Keller, 2011) conducted fatigue tests of multidirectional GFRP laminates under tension-tension (stress ratio: R = 0.1), tension-compression (R = -1) and compression-compression (R = 10). They revealed that fatigue strength was affected by both stress ratio and loading direction to the reinforcing fiber, and tension-compression fatigue strength was the lowest among the three types of stress ratio. They also measured residual stiffness during fatigue loading and reported that stiffness decreased with the number of loading cycles. This was called “stiffness degradation”, and many models have been proposed to predict it. (Andersen et al., 1996) proposed linear stiffness degradation model for the mid-region of fatigue life. (Whitworth, 1997) proposed another model which can predict the degradation for the early and mid-region of fatigue life. Recently, (Wu & Yao, 2010) proposed the model which covered all the fatigue life with single formula.

However, the fatigue strength and the stiffness degradation of GFRP may differ when woven roving bundles are used as reinforcement fibres. Woven roving FRP (glass fabric FRP) have been used in many civil structures (Roberto & Han, 2002)(Japan Society of Civil Engineers, 2011), but fatigue strength and stiffness degradation of them have not been studied well. In a previous study, authors focused on the model proposed by (Wu & Yao, 2010), and revealed that it could be applied to woven roving GFRP by setting appropriate experiment constants (Sato et al., 2022). However, compression fatigue behaviour of the woven roving GFRP has not been examined well. Therefore, this study conducted the compression-compression fatigue test with woven roving GFRP, and examined its fatigue strength and stiffness degradation. Furthermore, an attempt was made to reproduce the stiffness degradation under compression-compression fatigue using the theoretical model.

MATERIALS AND TESTING METHODS

Materials

In this study, hand lay-up molded GFRP was used as a specimen. The reinforcing fiber was roving glass cloth (Molymer SP, TH600AA 1000INT), which had equal amounts of fibers in two orthogonal directions. The resin matrix used was unsaturated polyester (DH Material, Sundoma 2915PT-M). Laminate structure was $[0/90]_{10}$, which meant it consisted of 10 layers of glass cloth with the same amount of fibres knitted in the 0° and 90° directions. Thickness of the laminate was 4.91 mm. Fiber volume fraction was 43.4%.

Static Test

Compression tests were conducted in accordance with JIS K 7018(Japan Standards Association (JSA), 2019). Static loading was applied to specimens of different lengths in order to obtain a compressive load capacity curve for the laminates. Dimensions of the specimens are shown in Figure 1. Five cases were prepared with the specimen length as a parameter. The specimens were 125 mm, 150 mm, 200 mm, 225 mm, and 250 mm in length. The specimen length 125 mm was specified in JIS standard, for which five specimens were prepared. Three specimens were prepared in the other cases. For static loading, an Amsler universal testing machine (maximum load: 1000 kN) and a Shimadzu servo pulser (maximum load: 50 kN) were used. In addition to measuring the load, the stress-strain relationship was measured from a strain gauge (FLAB-3, Tokyo Measuring Instruments Lab., 3 mm gauge length) placed in the center of the specimen.

Table 1 Size of specimens in previous studies (unit: mm)

Reference	Laminate	Length	Width	Thickness	Tab size
(Dadkhah et al., 1995)	3D-woven Carbon & Glass fiber	100	10	5.61-12.6	-
(Philippidis & Assimakopoulou, 2008)	GFRP $[90]_7$	145	25	6.16	50x25x2
(Uda et al., 2009)	CFRP$[45/0/45/90]_{4s}$	135	50	4	-
(Japan Standards Association (JSA), 2019)	-	125±1	25±0.5	>4	50x25x2

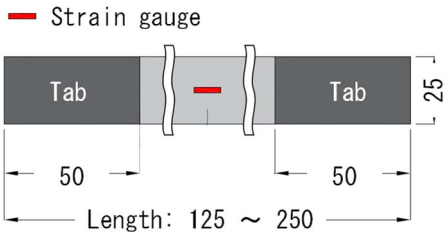

Figure 1 Static test specimen (unit: mm)

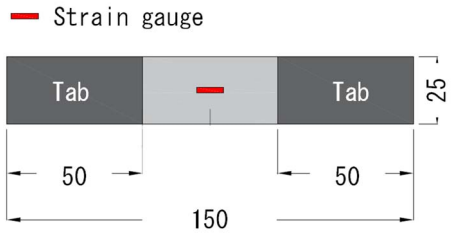

Figure 2 Fatigue test specimen (unit: mm)

Fatigue Test

Although there are previous studies that conducted compression fatigue tests of FRP, there is no general fatigue testing method(Baumann & Hausmann, 2021). Table 1 shows the dimensions of specimens used in previous studies and JIS standards. The specimen length of the static compression material test specified in JIS K 7018 is 125 mm. On the other hand, as can be seen from Table 1, specimen lengths of 100 mm to 145 mm were used in compression fatigue tests. In this study, the specimen size was set to 150 mm × 25 mm, as shown in Figure 2, for the purpose of visual observation and microscopic cross-sectional observation during the fatigue test.

Compression fatigue tests were also conducted under load control at room temperature using a Shimadzu servo pulser (maximum load of 50 kN). The loading frequency was set to 10 Hz and the stress ratio was set to 10. The previous study also conducted tension-tension fatigue test using woven roving GFRP under 10 Hz(Sato et al., 2022). It reported that temperature of the specimen did not exceed 40 degrees, so this study concluded that heating was negligible in the fatigue test under 10 Hz. In the compression fatigue test, the number of failure cycles (N_f) was recorded to obtain the S-N curve, and the fatigue test was interrupted at each specific loading cycles to measure the residual stiffness and observe the specimen. The residual stiffness was measured by static loading at a loading speed of 1 mm/min or less. Focusing on $500\ \mu\varepsilon < \varepsilon < 2500\ \mu\varepsilon$ from the stress-strain relationship obtained by static loading, the slope of this interval was calculated as the elastic modulus. The same type of strain gauge with static test and actuator displacement were used to measure the strain. Observations of the specimens were made by macro-observation and cross-sectional micro-observation using a microscope.

RESULTS AND DISCUSSIONS

Ultimate strength in the static compression test

Table 2 summarizes the compressive elastic modulus E and compressive strength σ_u obtained from each specimen length. Compressive elastic modulus and compressive strength were calculated by the following equations.

$$E = \frac{\sigma_{2500} - \sigma_{500}}{\varepsilon_{2500} - \varepsilon_{500}} \quad \text{Eq. 1}$$

$$\sigma_u = \frac{F}{A} \quad \text{Eq. 2}$$

where, σ: stress, ε: strain, σ_u: compressive strength, F: maximum compressive load, A: cross sectional area. The subscript in Eq. 1 represents the compressive strain (unit: $\mu\varepsilon$). From Table 2, it can be seen that the compressive modulus did not change regardless of the specimen length. The coefficient of variation for specimens with lengths of 125 mm and 250 mm exceeded 8%, but it was very small for other specimens. In addition, the compressive elastic modulus of the same kind of laminate in the previous study was 26.1-28.3 GPa (Myoga et al., 2017), which was very close to the value in this study.

Table 2 Summary of elastic modulus and compressive strength

Length (mm)	E-modulus (GPa)					Strength (MPa)				
	125	150	200	225	250	125	150	200	225	250
1	26.06	26.52	25.34	25.60	28.35	285.3	252.1	137.3	88.2	68.5
2	25.94	25.81	25.48	25.49	24.35	278.4	230.7	139.5	88.9	68.3
3	28.57	26.29	25.44	25.35	28.04	283.9	240.8	124.9	87.9	64.9
4	31.72	-	-	-	-	277.6	-	-	-	-
5	26.64	-	-	-	-	277.9	-	-	-	-
Mean	27.79	26.21	25.42	25.48	26.91	280.6	241.2	133.9	88.3	67.2
CV	8.78%	1.38%	0.29%	0.50%	8.26%	1.31%	4.43%	5.86%	0.54%	3.00%

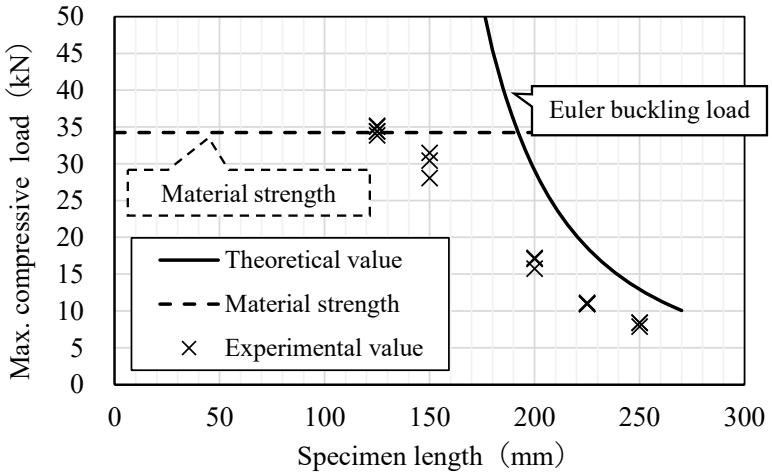

Figure 3 Maximum compressive load in static test ($K = 0.5$)

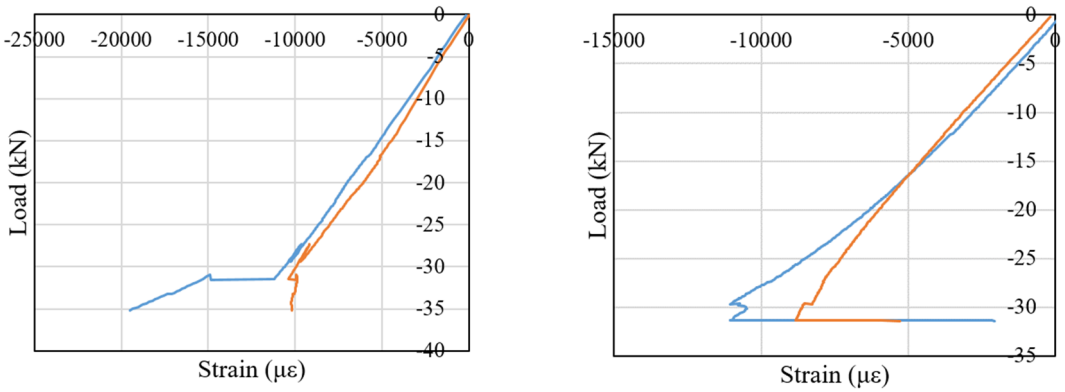

a) Specimen length: 125mm b) Specimen length: 150 mm

Figure 4 Load-Strain relationships

Focusing on the compressive strength, it can be seen from Table 2 that the compressive strength decreased as the specimen length increased. This can be explained using Euler's buckling theorem. Figure 3 shows a comparison of experimental and theoretical maximum compressive loads. Theoretical maximum load was calculated by the Euler's buckling theorem.

$$F = \frac{\pi^2 EI}{(Kl)^2} \qquad \text{Eq. 3}$$

where, I: moment of inertia, K: effective length factor, l: column length ($=$ specimen length $-$ 100). Effective length factor was set to 0.5 assuming fixed support at both ends. Figure 3 also shows the maximum load calculated from material compressive strength. Figure 3 shows that when the length of the specimen was 125 mm or 150 mm, the maximum compressive load was not achieved by Euler buckling but by material failure. However, maximum loads were different between 125-mm-long and 150-mm-long specimens. This is because the load increased even after partial material failure occurred when the specimen length was short. Figure 4 shows representative load-strain relationships of 125 mm and 150 mm cases. The strains were measured with the strain gauges installed on both sides of the specimens. The load-strain relationship in Figure 4 a) shows that 125-mm-long specimen exhibited a large difference in strain between the two sides at about -32 kN. This was due to partial material failure, but the load continued to increase by about 3 kN after the partial failure. Eventually, 125-mm-long specimen occurred total failure at -35 kN. On the other hand, for a specimen with a length of 150 mm, total failure occurred at -32 kN as shown in Figure 4 b). This made the difference in the maximum compressive load. Euler buckling occurred at the maximum load in the 200 mm, 225 mm, and 250 mm specimen length cases, but even in these cases the experimental maximum loads were lower than the theoretical values. The reason why the buckling

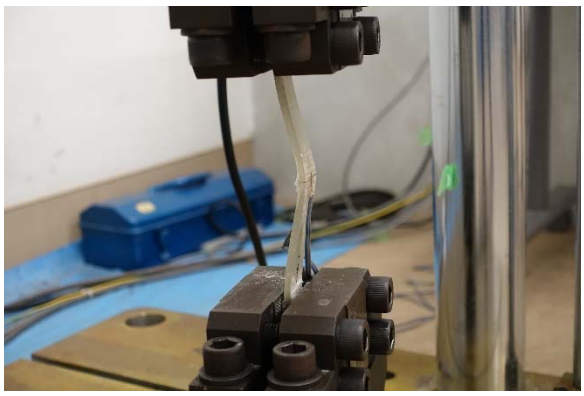

Figure 5 Buckling mode of 250-mm-long specimen

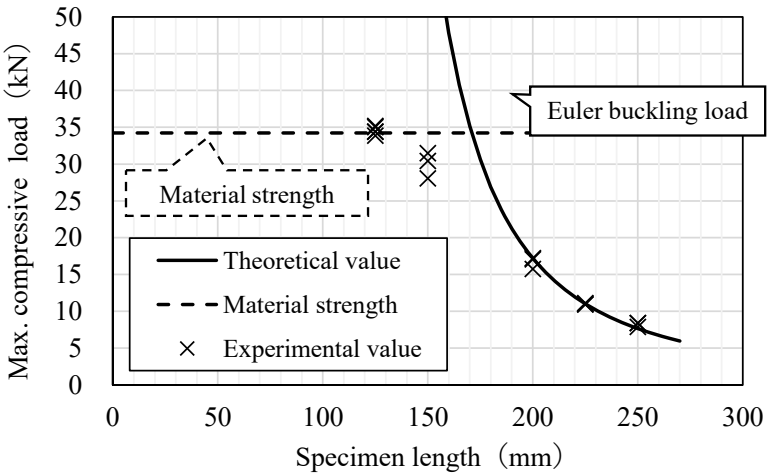

Figure 6 Maximum compressive load in static test ($K = 0.65$)

load in the experiment was lower than the theoretical value could be due to the initial imperfection or the jig was not fully fixed. Figure 5 shows failure mode of a 250-mm-long specimen.
Although the test piece in Figure 5 was held by the upper and lower jigs, there was a distance between the crosshead and the upper jig. The rotation angle of the upper part of the test piece could not be restrained rigidly during loading, as shown in Figure 5. Figure 6 shows the comparison between the experimental and theoretical values with an effective length factor of 0.65. Figure 6 shows that when the effective length coefficient was set to 0.65, the theoretical and the experimental values were in good agreement. The effective length coefficient is 0.7 for the one-sided fixed - one-sided pin supported condition. The effective length coefficient of 0.65 assumed in Figure 6 was between the two end-fixed conditions and the fixed-pin-supported condition. This implies that deflection angle was not fixed rigidly on one side.

Compressive fatigue strength

Figure 7 shows the S-N curves obtained from the compression fatigue tests, and Table 3 summarizes the number of fracture cycles. The vertical axis of Figure 7 is the ratio of the minimum loading stress σ_{min} (maximum compressive stress) to the static strength σ_u. Here, the compressive strength of the 125-mm-long specimen in Table 2 was used as σ_u. Table 3 lists not only the minimum loading stresses but also the loading stress range. As shown in Figure 7, the compressive fatigue strength was able to be expressed as a straight line on the S-N curve, and no clear fatigue limit appeared until 10 million cycles. The 10 million cycles fatigue strength of this study was 40% of the static strength. Nine of the ten specimens exhibited failure mode like that shown in Figure 8, while fatigue failure occurred at the aluminium tab reinforcement in one specimen, as shown in Figure 9. However, there was no significant difference in fatigue strength between these failure modes.

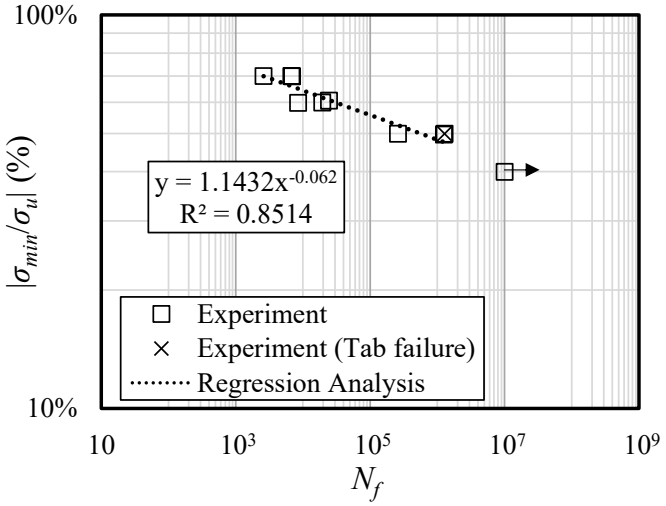

Figure 7 S-N curve of compressive fatigue tests

Table 3 Summary of compressive fatigue strength

Cycles to Failure: N_f	$\lvert\sigma_{min}\rvert$ (MPa)	$\lvert\sigma_{min}/\sigma_u\rvert$	$\Delta\sigma$ (MPa)	$\lvert\Delta\sigma/\sigma_u\rvert$	Note
6,899	196	70%	176	63%	
6,736	196	70%	176	63%	
2,603	196	70%	176	63%	
24,309	170	61%	153	55%	
19,406	168	60%	151	54%	
8,494	168	60%	151	54%	
1,256,423	139	50%	125	45%	
259,673	140	50%	126	45%	
1,273,983	140	50%	126	45%	Tab failure
10,000,000	112	40%	101	36%	Did not fail

Figure 8 Compressive fatigue failure

Figure 9 Tab failure

Figure 10 shows the comparison of tensile (R = 0.1) and compressive (R = 10) fatigue strength. Tensile fatigue strength shown in Figure 10 were referred from the previous study which used $[0/90]_4$ as specimens (Sato et al., 2022). It can be seen from Figure 10 that tensile fatigue strength was slightly larger than those of compression in the short fatigue life region ($N_f < 10^5$). On the other hand, they exhibited almost the same fatigue strength in the long fatigue life region ($N_f > 10^5$).

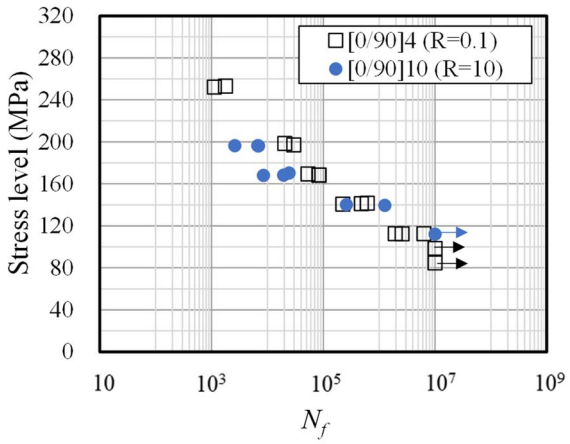

Figure 10 Comparison of tensile (R = 0.1) and compressive (R = 10) fatigue strength

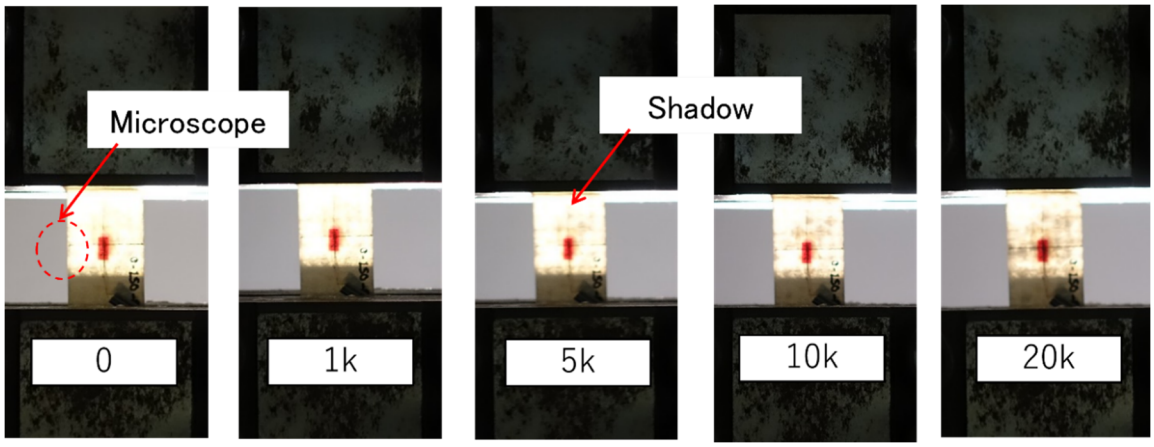

Figure 11 Progression of fatigue damage in macro observation
($|\sigma_{min}/\sigma_u| = 60\%$, $N_f = 24{,}309$)

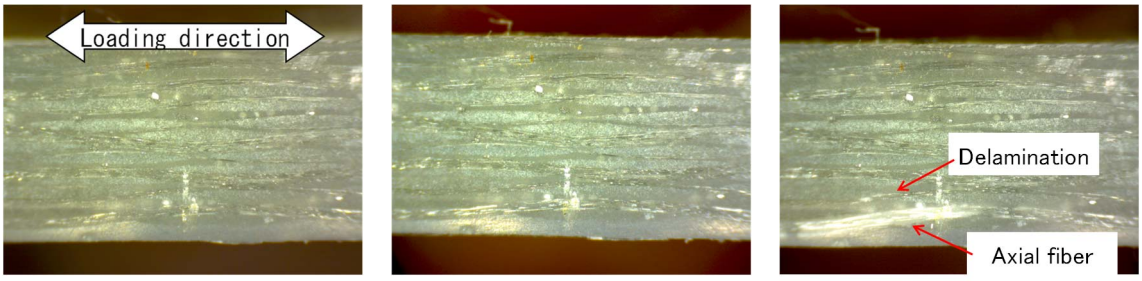

a) 0 cycles b) 5,000 cycles c) 20,000 cycles

Figure 12 Progression of fatigue damage in micro observation
($|\sigma_{min}/\sigma_u| = 60\%$, $N_f = 24{,}309$)

Vassilopoulos & Keller (2011) conducted fatigue tests on $[0/(45)_2/0]_T$ GFRP laminates and reported that it showed lower compressive fatigue strength than tensile fatigue strength in the short fatigue life region. They discussed that lower static compressive strength than tensile strength resulted in the low compressive fatigue strength. However, tensile strength of the laminates used in (Sato et al., 2022) was 281.1 MPa, which was almost the same as compressive strength (σ_u = 280.6 MPa) in this study. The reason why fatigue strength was different between tension-tension and compression-compression loading may be from the progression of fatigue damage, which will be discussed in the following section. Vassilopoulos & Keller also conducted tension-compression fatigue tests with R = -1 and reported that the fatigue strength was clearly lower than that of R = 0.1 or R = 10. In this study, all fatigue tests were conducted by single side loading fatigue test because dead load is always applied on

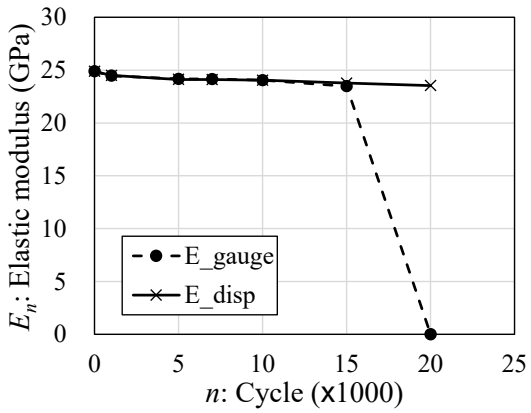

Figure 13 Compressive modulus history

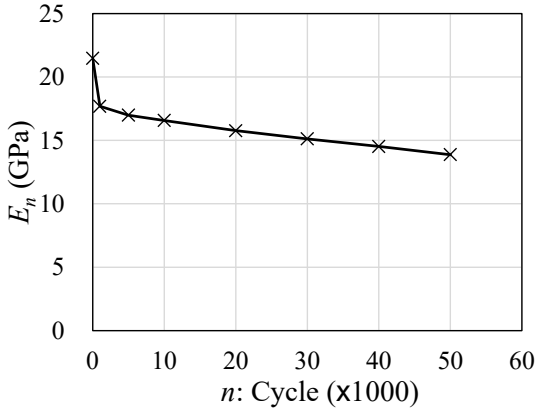

Figure 14 Tensile modulus history (Sato et al., 2022)

the bridge while it is in service as a road bridge, but a different S-N curve may be obtained in case of tension-compression fatigue loading.

Progression of fatigue damage

Figure 11 shows the change in appearance as the number of fatigue loading cycles increases. The number shown in Figure 11 indicates the number of loading cycles. In the macro-observation, fatigue damage was observed using transmitted light. When delamination occurred at 5,000 cycles, transmitted light was diffusely reflected and was observed as a shadow area. This delamination area expanded as the number of loading cycles increased. The cross section of the area indicated by the red circle in Figure 11 was observed using an optical microscope. Figure 12 shows the results of the microscope observation. As shown in Figure 12, the delamination was observed at 20,000 cycles in the microscope view. The macro-observation confirmed the delamination at 5,000 cycles as shown in Figure 11, but it was not seen in Figure 12. This is because the delamination initiated around the center of the specimen and emerged near its edge at 20,000 cycles. It was also observed that some of the glass fiber bundles aligned in the loading direction were discolored at 20,000 cycles. This implies the weakening of the adhesion between the glass fibers constituting the fiber bundles by repeated compressive stresses. On the other hand, Figure 12 does not show any cracks in the resin matrix which propagate in the direction perpendicular to the loading. Previous study which conducted tension-tension fatigue tests reported that tensile fatigue damage of woven roving GFRP progressed as follows: 1) resin matrix cracks perpendicular to the loading, 2) delamination, and 3) glass fiber fracture in loading direction (Sato et al., 2022). However, the macro and micro-observations in this study suggested that compressive fatigue damage initiated as the delamination and the weakening of adhesion in the fiber bundles in the loading direction. Then, most of fatigue life was spent in progression of delamination. These differences of fatigue damage progression between tension and compression were thought to have resulted in the different fatigue life shown in Figure 10. The resin matrix cracks observed in tensile fatigue damage opened perpendicular to the loading direction, which meant mode I crack occurred due to tension force. On the other hand, in compression fatigue, this kind of matrix cracks did not initiate because no tension force was applied inside the specimen.

Stiffness degradation due to compressive fatigue loading

The relationship between the number of loading cycles n and the compressive modulus E_n is shown in Figure 13. In Figure 13, “E_gauge” means the compressive modulus measured by strain gauges (3 mm gauge length), and “E_disp” is the modulus by the actuator displacement. When E_disp was calculated, a constant coefficient was used to compensate the difference between E_gauge and E_disp at 0 cycles. As can be seen in Figure 13, the compressive modulus decreased slightly with the increasing number of loading cycles. Up to 15,000 cycles, E_gauge and E_disp showed almost the same value, but at 20,000 cycles, only E_gauge plummets to 0 GPa. This was due to strain gauge

failure. In other cases as well, the compressive modulus could not be obtained from the strain gauges in the region of large number of cycles. The relationship between the number of cycles and the compressive modulus showed an almost linear decrease up to 20,000 cycles. This tendency was different from those of tensile fatigue loading. Figure 14 shows the tensile modulus history which was obtained during the tension-tension fatigue test (Sato et al., 2022). It can be seen from Figure 14 that in the case of tension-tension fatigue, the tensile modulus decreased rapidly in the early stages of loading cycles. The subsequent decrease of tensile modulus was linear, as in the case of compression-compression fatigue, but the slope was greater in tension-tension fatigue. This different tendency of the stiffness degradation may be related to the progression of the fatigue damage. That is, in tension-tension fatigue, matrix cracks were initiated in the early stage of loading cycles, at which time the elastic modulus dropped rapidly. On the other hand, the elastic modulus decreased almost linearly with the number of cycles when delamination developed in the specimen.

MODELING OF COMPRESSIVE STIFNESS DEGRADATION

The residual compressive modulus for all cases are shown in Figure 15. The horizontal and vertical axes of Figure 15 are non-dimensionalised by the fatigue life (N_f) and the initial compressive modulus (E_0), respectively. The legend in Figure 15 represents the ratio of the applied maximum compressive stress to the compressive strength ($|\sigma_{min}/\sigma_u|$). It can be seen from Figure 15 that the compressive modulus decreased almost linearly in all cases, irrespective of the applied stress. This study could not measure the residual compressive modulus in $n/N_f > 0.9$ because the modulus was measured through static loading when fatigue loading was paused at certain loading cycles. However, (Vassilopoulos & Keller, 2011) conducted compression-compression fatigue test using different laminate structure, and reported that they did not confirm sharp stiffness degradation even just before the fatigue failure. Therefore, this research regarded the stiffness degradation in compressive modulus as linear degradation, and formulated as follows:

$$E_n = E_0\left(1 - C\frac{n}{N_f}\right) \qquad \text{Eq. 4}$$

where, C: constant. The constant C was calculated to be 9.77×10^{-2} from regression analysis. In previous studies, a stiffness degradation model had been proposed focusing on tensile fatigue damage, which stated that the stiffness decreases linearly with the number of cycles in the middle of the fatigue life (Andersen et al., 1996). However, the present study is novel in that the linear degradation model can be applied to the entire fatigue life for compressive fatigue damage, assuming that the development of delamination is dominant throughout the fatigue life. The model and experimental values are compared in Figure 15. It was verified that the proposed model and experimental results agreed well especially in early to middle stage of fatigue life.

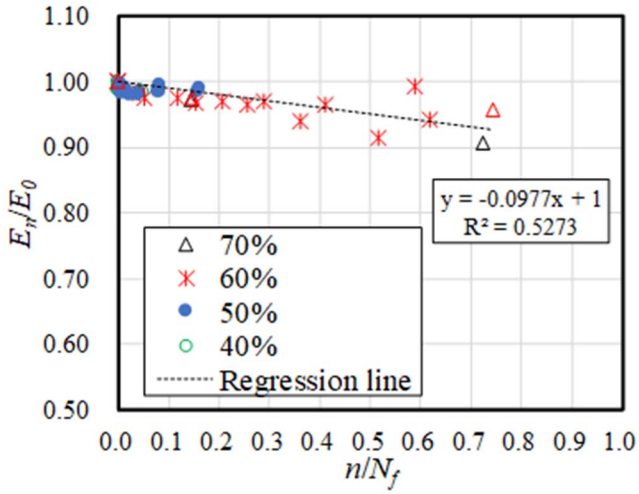

Figure 15 Comparison of proposed model and the experimental value of residual stiffness

CONCLUSION

This study conducted compressive static and fatigue test using woven roving GFRP laminate. Residual compressive modulus was measured through static loading which was conducted at certain number of loading cycles. The following conclusions can be drawn:

1. Static loading was carried out for several specimen lengths in the compression tests to obtain load capacity curves for the materials. Although the compressive load carrying capacity obtained from the experiments was smaller than the Eulerian buckling load due to imperfections and the boundary conditions of the fixture, the two agreed well when the effective length factor was set to 0.65.
2. The compressive fatigue strength was able to be expressed as a straight line on a double logarithmic graph. The compressive stress corresponding to the 10^7 cycles fatigue strength was 112 MPa, which is 40% of the static strength. Comparison of the S-N curves for tension-tension and compression-compression fatigue showed that compressive fatigue showed lower fatigue strength in the low-life region, but they agreed well in the medium to high-life region.
3. Micro observations showed few cracks in the matrix resin in the compression fatigue test. However, the delamination was observed in macro and micro-observations using transmitted light, suggesting that delamination was dominant in compression fatigue damage.
4. The residual compressive stiffness was formulated assuming a linear decrease up to fatigue failure. The proposed model was in good agreement with the experimental data.

ACKNOWLEDGEMENT

This study was supported by JSPS KAKENHI Grant Number JP22J15081.

CONFLICT OF INTEREST

The authors declare that they have no conflicts of interest associated with the work presented in this paper.

DATA AVAILABILITY

Data on which this paper is based is available from the authors upon reasonable request.

REFERENCES

Andersen, S. I., Brøndsted, P., & Lilholt, H. (1996). *Fatigue of polymeric composites for wingblades and the establishment of stiffness-controlled fatigue diagrams*.

Bank, L. C. (2007). Composites for Construction: Structural Design with FRP Materials. In *Composites for Construction: Structural Design with FRP Materials*. https://doi.org/10.1002/9780470121429

Baumann, A., & Hausmann, J. (2021). Compression Fatigue Testing Setups for Composites—A Review. In *Advanced Engineering Materials* (Vol. 23, Issue 2). Wiley-VCH Verlag. https://doi.org/10.1002/adem.202000646

Behrends, M. A., & Brayshaw, T. (2012). *Testing and Health Monitoring of an Integrally Molded Fiber Reinforced Polymer Bridge*.

Dadkhah, M. S., Coxt, B. N., & Morris, W. L. (1995). COMPRESSION-COMPRESSION FATIGUE OF 3D WOVEN COMPOSITES. In ~ *Pergamon Acta metall, mater* (Vol. 43, Issue 12).

Hollaway, L. C., & Head, P. R. (2001). Chapter 8 - Applications in advanced polymer composite constructions. In L. C. Hollaway & P. R. Head (Eds.), *Advanced Polymer Composites and Polymers in the Civil Infrastructure* (pp. 221–286). Elsevier Science Ltd. https://doi.org/https://doi.org/10.1016/B978-008043661-6/50010-3

Japan Society of Civil Engineers. (2011). *Guidelines for Design and Construction of FRP footbridges*.

Japan Standards Association (JSA). (2019). *Fiber-reinforced plastic composites- Determination of compressive properties in the in-plane direction*.

Myoga, M., Kader, A., Kitane, Y., Itoh, Y., & Hibi, H. (2017). EXPERIMENTAL STUDY ON STRENGTH EVALUATION OF SINGLE-BOLTED CONNECTIONS OF HAND LAY-UP

GFRP MEMBERS. *Journal of Japan Society of Civil Engineers, Ser. A1 (Structural Engineering & Earthquake Engineering (SE/EE))*, *73*(5), II_62-II_73.

Philippidis, T. P., & Assimakopoulou, T. T. (2008). Strength degradation due to fatigue-induced matrix cracking in FRP composites: An acoustic emission predictive model. *Composites Science and Technology*, *68*(15–16), 3272–3277. https://doi.org/10.1016/j.compscitech.2008.08.020

Roberto, L.-A., & Han, X. (2002). Structural Characterization of Hybrid Fiber-Reinforced Polymer-Glulam Panels for Bridge Decks. *Journal of Composites for Construction*, *6*(3), 194–203. https://doi.org/10.1061/(ASCE)1090-0268(2002)6:3(194)

Sato, A., Kitane, Y., Hibi, H., Goi, Y., & Sugiura, K. (2022). FATIGUE STRENGTH AND STIFFNESS DEGRADATION OF HAND LAY-UP GFRP. *Journal of Japan Society of Civil Engineers, Ser. A1 (Structural Engineering & Earthquake Engineering (SE/EE))*, *78*(5), II_54-II_65.

Siwowski, T., Kaleta, D., & Rajchel, M. (2018). Structural behaviour of an all-composite road bridge. *Composite Structures*, *192*, 555–567. https://doi.org/10.1016/j.compstruct.2018.03.042

Uda, N., Ono, K., & Kunoo, K. (2009). Compression fatigue failure of CFRP laminates with impact damage. *Composites Science and Technology*, *69*(14), 2308–2314. https://doi.org/10.1016/j.compscitech.2008.11.031

Vassilopoulos, A. P., & Keller, T. (2011). *Fatigue of Fiber-reinforced Composites*. Springer London. https://doi.org/10.1007/978-1-84996-181-3

Whitworth, H. A. (1997). A stiffness degradation model for composite laminates under fatigue loading. In *Composite Smctures* (Vol. 40, Issue 2).

Wu, F., & Yao, W. X. (2010). A fatigue damage model of composite materials. *International Journal of Fatigue*, *32*(1), 134–138. https://doi.org/10.1016/j.ijfatigue.2009.02.027